Fabrication of 3D scaffolds reproducing intestinal epithelium topography by high-resolution 3D stereolithography

Justine Creff, Rémi Courson, Thomas Mangeat, Julie Foncy, Sandrine Assié-Souleille, Christophe Thibault, Arnaud Besson, Laurent Malaquin

Fabrication of 3D scaffolds reproducing intestinal epithelium topography by high-resolution 3D stereolithography

Justine Creff[1,2], Rémi Courson[2], Thomas Mangeat[1], Julie Foncy[2], Sandrine Souleille[2], C. Thibault[2], Arnaud Besson[1*] and Laurent Malaquin[2*]

[1]LBCMCP, Centre de Biologie Intégrative, Université de Toulouse, CNRS, UPS, 31062 Toulouse Cedex, France.

[2]LAAS-CNRS, Université de Toulouse, CNRS, F-31400, Toulouse, France

[*]these authors contributed equally to this work

Corresponding authors:

Arnaud Besson
LBCMCP UMR5088 CNRS - Université Paul Sabatier-Toulouse III,
Centre de Biologie Intégrative, CBI FR3743
118 route de Narbonne
31062 Toulouse cedex 9, France
Email: arnaud.besson@univ-tlse3.fr
Tel: +33 (0)561558486

Laurent Malaquin
LAAS-CNRS, Université de Toulouse, CNRS, INSA, Toulouse, France.
7 avenue du Colonel Roche
31031 Toulouse Cedex 4 – BP 54200
Email: laurent.malaquin@laas.fr
Tel: +33 (0)561336384

Abstract

The small intestine is a complex tissue with a crypt/villus architecture and high tissue polarity. Maintenance of tissue integrity and function is supported by a constant renewal of the epithelium, with proliferative cells located in the crypts and differentiated cells migrating upward to the top of villi. So far, most *in vitro* studies have been limited to 2D surfaces or 3D organoid cultures that do not fully recapitulate the tissue 3D architecture, microenvironment and cell compartmentalization found *in vivo*. Here, we report the development of a 3D model that reproduces more faithfully the architecture of the intestinal epithelium *in vitro*. We developed a new fabrication process combining a photopolymerizable hydrogel that supports the growth of intestinal cell lines with high-resolution stereolithography 3D printing. This approach offers the possibility to create artificial 3D scaffolds matching the dimensions and architecture of mouse intestinal crypts and villi. We demonstrate that these 3D culture models support the growth and differentiation of Caco-2 cells for 3 weeks. These models may constitute a complementary approach to organoid cultures to study intestinal homeostasis by allowing guided self-organization and controlled differentiation, as well as for *in vitro* drug screening and testing.

Keyword:

3D printing, scaffold, intestine, crypt, villus, hydrogel

Introduction

The primary function of the intestinal tract is the digestion and absorption of nutrients. To maintain optimal function and tissue integrity, the intestinal epithelium is constantly renewed. The epithelium of the small intestine is organized into a large number of "crypt-villus" units. Villi are finger-like structures covered by a simple epithelium of differentiated cells projecting into the intestinal lumen to maximize nutrient absorption. The base of each villus is surrounded by several invaginations, called crypts of Lieberkühn. The constant renewal of the epithelium is driven by intestinal stem cells (ISCs) that reside at the crypt base [1-3]. ISCs proliferate and produce progenitors, called transit-amplifying cells, localized just above the stem cell zone in the crypt. These progenitors undergo several rounds of division and migrate along the crypt-villus axis while they terminally differentiate into different cell types, including enteroendocrine, tufts and goblet cells, and enterocytes [1, 3, 4]. Stem cell self-renewal and progenitor differentiation are supported by the crypt microenvironment, or niche. This microenvironment changes along the crypt-villus axis and determines the balance between proliferative and differentiation signals [3]. For instance, the Wnt, Notch and Noggin growth factors are present in decreasing gradients from the crypt bottom [5, 6]. Additional signals provided by the extracellular matrix (ECM), microbiota and immune cells are also important for ISC maintenance and progenitor differentiation [3, 7]. Despite numerous studies, the exact mechanisms governing intestinal homeostasis remain poorly understood, possibly due to the lack of *in vitro* models to grow and study ISCs and their progeny.

Recent progress in stem cell technology has allowed developing three-dimensional (3D) cultures from primary mouse and human adult ISCs [8-10]. In these cultures, cells self-organize into intestinal organoids exhibiting self-renewing crypt compartments, with proliferative cells that differentiate to give flat "villi-like" domains. While these 3D systems recapitulate the heterogeneity of the intestinal tissue *in vitro,* they present several limitations, notably their spherical architecture and lack of lumen. Moreover, these structures cannot support the formation of signaling gradients and mechanical forces, and therefore do not fully recreate the native microenvironment [11].

To address these limitations, several studies reported the development of new engineered culture systems to study the intestinal epithelium [12]. In particular, recent advances in

microfabrication technologies and biomaterials made possible the development of new 3D *in vitro* systems more physiologically relevant to study the intestinal epithelium [11, 13, 14]. Most of these systems use Caco-2 cells as tissue mimic. Caco-2 are human colorectal adenocarcinoma cells that spontaneously differentiate into a polarized epithelium exhibiting characteristics similar to small intestine enterocytes upon reaching confluence [15]. In order to recreate the architecture of the intestinal epithelium, various 3D micro-patterned scaffolds mimicking intestinal villi [16-21] or crypts [22] have been developed, mostly using molding or lithography technologies.

These studies have clearly demonstrated the interplay between cell differentiation, polarization and 3D microenvironment. Recently, a 3D model reproducing the crypt/villi architecture and biochemical gradients using micro-molded cross-linked collagen was developed to culture primary human intestinal cells [23, 24]. This model has shown that 3D topology, in addition to other physical and chemical cues, is a key factor to promote cell differentiation and polarization. However, due to limitations in the resolution and/or complexity of the fabrication techniques, many of these 3D models still fail to fully recapitulate or accurately control the topology of crypt/villi compartments. In this work, we investigated the capabilities of 3D printing to improve the resolution and complexity of topographies accessible for scaffold fabrication compared to molding technologies. Recent advances in additive manufacturing technologies such as extrusion printing, inkjet printing or laser assisted printing now allow printing biocompatible materials with full flexibility on the design and shape. An attractive method for bioprinting is stereolithography (SLA) that uses a light-induced polymerization process [25, 26]. This approach offers the possibility to rapidly create complex objects at high resolution using a large range of photosensitive materials including rigid photoresists or synthetic hydrogels [27, 28]. This technology has been used for cell culture, either for the fabrication of scaffolds or for direct printing of cells encapsulated in ECM [29, 30]. However, most of the approaches reported so far are still limited by the resolution of the printing technologies, typically above 50 µm. Two-photons based techniques may offer a resolution in the sub-micrometer range but are still strongly limited by the printing speed and by the maximum sample volume that is accessible. We recently reported a new 3D SLA printing technology that compensates for these limitations [31]. It combines a resolution of 5 µm in x, y and z and the possibility to print large objects (maximum 10(x) x 10(y) x 5(z) cm^3). This resolution enables to print scaffolds mimicking the architecture and dimensions of the intestinal epithelium.

The choice of the material used to create the scaffold is critical. To improve biocompatibility and relevance for bioengineered systems, various materials have been investigated, such as Polydimethylsiloxane (PDMS), SU-8 epoxy resin, collagen, or silk [16, 17, 19-22]. While natural materials are very effective to support cell growth and differentiation, they are often not completely defined and contain animal-derived products that preclude clinical applications. Moreover, ECM such as collagen are mostly biodegradable and the 3D topography is not conserved in long-term cultures [18]. A common alternative for tissue engineering is the use of synthetic polymers such as poly(ethylene)glycol diacrylate (PEG-DA) or polyacrylamide [32, 33]. These synthetic hydrogels are more controllable and offer more flexibility to control mechanical and chemical properties in a reproducible manner. Moreover, these materials are compatible with 2D/3D fabrication through photolithography based approaches [30, 34, 35]. Beyond their reproducibility, another advantage of synthetic materials is the possibility to modify them, allowing their tuning with degradation and/or adhesion sites or even growth factors [32, 36-38]. For instance, to support cell growth and colonization, adhesion ligands such as RGD peptides or laminin can be grafted to the hydrogel [39]. Synthetic hydrogels based on poly(ethylene)glycol polymer (such as PEG-4MAL or 8arm-PEG4) have been used to replace Matrigel in 3D intestinal organoid cultures to improve the control and reproducibility over matrix physicochemical properties [40, 41]. Here, we developed a novel photosensitive biomaterial based on an intricate network composed of PEG-DA and acrylic acid polymer chains that allows cell adhesion and proliferation. Whereas many material formulations may require complex synthesis or numerous functionalization steps, this material is simple to prepare and can be functionalized easily with ECM proteins to improve cell attachment and proliferation. Moreover, it combines a high optical transparency for microscopy imaging with tunable stiffness properties. Using high-resolution stereolithography technology, we 3D printed this material with a micrometric resolution and successfully reproduced the topography and dimensions of the different compartments of the mouse intestinal epithelium. Finally, we showed that this culture system supports the growth of Caco-2 cells and allows the formation of a polarized and differentiated epithelium in three dimensions.

Experimental section

Cell culture

Caco-2 cells were cultivated in DMEM 4.5 g/L glucose (Sigma, D6429) supplemented with 20% Fetal Bovine Serum (FBS, Life Technologies, 10270106), 0.1 mM non-essential amino acids (Sigma, M7145) and 2 µg/mL penicillin/streptomycin (Sigma, P4333). SW480 cells were cultivated in RPMI 2 g/L glucose (Sigma, R8758) supplemented with 10% FBS, 0.1 mM non-essential amino acids, 2 µg/mL penicillin/streptomycin and 2.5 g/L D-Glucose (Sigma, G7021). All cells were grown at 37°C and 5% CO_2. For cell culture on 2D hydrogels, Caco-2 or SW480 cells were seeded at a density of 20,000 cells.cm^{-2} and grown for 6 days with medium changes every 2-3 days. For 3D cultures or control 2D cultures, Caco-2 cells were plated at a density of 75,000 cells.cm^{-2} in conditioned media (culture supernatant) and kept in culture for up to 3 weeks with medium changed every 2-3 days.

Hydrogel preparation

Hydrogels were prepared as described previously [42]. The photoinitiator Phenylbis(2,4,6-trimethyl-benzoyl)phosphine oxide (Irgacure 819, Sigma, 511447) was dissolved at 0.1% (wt/vol) in PEG-DA MW 700 (Sigma, 455008). To prepare hydrogels, the different components were mixed in a conical tube: PEG-DA 700 (30-60%) (vol/vol) containing the photoinitiator, 30% acrylic acid (Sigma, 147230) (vol/vol) supplemented or not with either 250 µg/ml fibronectin (Corning, 356008), 50 µg/ml laminin (Sigma, L2020) or 1% collagen-1 (Sigma, C4243), the volume was then completed with culture medium (10-40%) (vol/vol). Ultraviolet crosslinking was performed using a UV lamp (365 nm, 12 W) or the Dilase 3D printer (Kloé, France). Polymerized hydrogels were washed overnight in culture medium prior to cell seeding.

3D printing of intestinal scaffold

Intestinal scaffolds were printed by stereolithography with a Multiresolution Dilase 3D setup (Kloé SA, France) (Fig.1). This equipment and its performances have been described in our previous work [31]. STL file, made with CAO 3D software, was sliced using the 3D slicer software (Kloé). The first 200 µm (crypt part) were sliced in 50 µm thick layers (four layers) and printed with a 5 µm spot size, while villi were sliced in 20 µm layers (35 layers) and printed with a 20 µm spot size. The total dimensions of the sample were 4x4x0.7 mm^3 for 500µm high villi

and 4x4x1.7 mm^3 for 1500µm high villi (Fig. 3). To ensure adhesion of the PEG-DA hydrogel during the 3D printing process, a DS-3000 (DWS, Italy) substrate of 1x1x0.05 cm^3 was prepared by 3D printing using DWS 29J+ or B9 creator® systems. Indeed, just after the development step, the DS-3000 surface (last printed layer) is still reactive because of the uncrosslinked polymer chains that was in contact with the PDMS in the printer vat [31]. Consequently, PEG-DA can create covalent bonds with pending acrylate functions on the DS-3000 surface. Regarding the parameters employed for the production of the 3D scaffold, a pedestal of 50 µm was first fabricated with 100% laser power and 15 mm/s writing speed. This pedestal allowed a strong adhesion on substrate and ensured parallelism between the substrate and the top of the tank. Then, a laser power of 100% and a writing speed of 20 mm/s were set to fabricate the rest of the scaffold. Total fabrication time of the structure was 12 h. After laser writing, the sample was removed from the building table and developed by two successive water baths, the sample was kept in water to prevent dehydration and deformation of the structure. Before cell seeding, 3D scaffolds were sterilized using UV light (365 nm, 12 W) for 20 min and washed 3 times with culture medium.

Immunofluorescence

Cells were rinsed with PBS and fixed with 2% PFA for 20 min at 37°C. Cells were permeabilized using PBS-0.2% Triton X-100 for 3 min. After three 5 min washes in PBS, cells were incubated with primary antibodies diluted in PBS + 3% BSA + 0.05% Tween 20 + 0.08% sodium azide for 1 h at 37 °C or with phalloïdin conjugated to FITC or rhodamine (Interchim) at 1/500 for 30 min at 37°C. Primary antibodies used for immunofluorescence were: Mouse anti Pan-cytokeratin (Cell signaling, C11 #4545 [1/100]), Goat anti Villin (Santa Cruz Biotechnology, C-19, sc-7672 [1/50]) and Mouse anti β-catenin (BD Biosciences #610153 [1/200]). After three 5 min washes in PBS, cells were incubated for 30 min at 37°C with Cy2-conjugated secondary antibodies (Jackson ImmunoResearch) at 1/400 dilution. For F-actin co-staining, phalloïdin was added to secondary antibody solution. Cells were then rinsed three times 5 min in PBS, with the first wash containing Hoechst 33342 (0.1 µg/mL) or DRAQ5 (Thermo Fisher Scientific) at 1/1000 for nuclear DNA staining.

Alkaline phosphatase activity

Alkaline phosphatase activity was assessed with Blue Alkaline Phosphatase (Blue AP) Substrate kit (Vector Laboratories, SK-5300), according to the manufacturer's protocol. Briefly, living cells were rinsed with PBS and incubated for 30 min at 37°C with Blue AP substrate in Tris Buffer (150 mM, pH 8.4), rinsed with PBS and fixed with 4% PFA for 20 min at 37°C.

Atomic Force Microscopy (AFM)

AFM measurements were performed using Borosilicate Glass Particle (10 µm) on silicon nitride cantilevers (PT.BORO.SN.10, Novascan Technologies) with a nominal spring constant of 0.06 N/m mounted on a NanoWizard III AFM (JPK Instruments) coupled to an inverted optical microscope (Axiovert 200, Carl Zeiss). To ensure reproducibility in force application and measurement, the cantilever sensitivity and spring constant were calibrated before each experiment using the JPK Instrument software using the thermal noise method. Force-distance curves were recorded in contact mode in liquid at 2 Hz (1 s per approach-retract force curve) with an applied force of 1 nN. Each hydrogel was tested at 4 locations with about 250 force curves acquired per location and 512 data points per curve.

Surface topography imaging was performed by AFM using a MLCT cantilever (Bruker) with a nominal spring constant of 0.07 N/m on a NanoWizard III AFM (JPK Instrument). Imaging 3D scaffold was realized at the top of the villi.

Image acquisition and analysis

Images of 2D cultures and brightfield images of 3D scaffolds and 2D hydrogels were captured on a Nikon Eclipse 90i microscope using a Nikon DS-Qi2 HQ camera or a DS-U3 color camera (Nikon) and NIS Element BR software.

Two-photon confocal imaging was performed using an upright multiphoton Zeiss LSM 7MP microscope equipped with a pulsed laser adjustable from 690 to 1080 nm and a 20X plan-Apo water immersion objective.

Confocal images were acquired on an upright Leica SP8 confocal microscope equipped with 2 PMT detectors and 488 nm, 552 nm and 638 nm diodes and a 25X physio objective.

For Light Sheet Fluorescence Microscopy, samples were first embedded in 1% low-melt agarose and specimens were imaged from the side with a 2X objective and a 561 nm laser.

SEM imaging was performed using a Hitachi S-3700 microscope with an acceleration voltage ranging from 1,5 kV to 2 kV.

Dynamic Speckle Imaging (DSI) [43] was performed for whole 3D epithelium high-resolution imaging. This technique produces fast 3D resolution imaging and combines high sectioning properties together with high lateral resolution. The method consists in producing hundreds (200 during the experiments performed in this work) of speckle illumination in each acquisition plane along the depth of the sample. A post treatment combining pre-filtering of each raw image with statistical analysis based on the square root of the variance was made with a homemade Matlab software. This process enables a confocal imaging of the entire biological object and preserves the lateral resolution up to 700 µm depth. Indeed, speckle illumination is known to be poorly sensitive to optical aberrations or scattering [44] and this reduces problems of working distance (a 0.14 NA microscope lens was used for the collection of fluorescence emission). All images were treated and analyzed with the Fiji Software.

Statistical analyses

Statistical analyses were performed on three independent experiments using the GraphPad Prism 6.0 Software. Differences between groups were considered statistically significant if $p < 0.05$. Data were compared using one-way ANOVA followed by Bonferroni correction for multiple comparisons. Data are presented as mean +/- SEM.

Results

Development of a new photosensitive hydrogel

The goal of this study was to develop a new 3D model of intestinal epithelium using high-resolution 3D printing (Fig. 1). One of the main challenges was to develop a material compatible with cell culture adapted to a 3D printing process and offering optical properties suitable for fluorescence microscopy imaging. We selected PEG-DA polymer as a base material to form hydrogel through radical polymerization in presence of photoinitiator [45]. PEG-DA hydrogels were previously reported to constitute poor substrates for cellular adhesion due to their protein repelling properties [32, 39]. To improve cellular adhesion, we investigated the addition of acrylic acid to PEG-DA to form composite hydrogel networks. Acrylic acid reacts with PEG-DA and provides free carboxylic groups that negatively charge the resulting hydrogel. These groups were shown to promote protein adhesion at neutral pH (Fig. 2A) [42]. After polymerization, the remaining acrylic acid species that did not react were extracted from the polymer matrix by several washes in culture medium to reestablish a neutral pH in the scaffold and avoid potential toxicity on cell cultures. Cell adhesion and biocompatibility of PEG-DA hydrogels complemented or not with acrylic acid and/or ECMs were evaluated after 6 days of culture with SW480 colorectal cancer cells (Fig. 2B, C). While the presence of fibronectin in pure PEG-DA hydrogel was not efficient to promote cell adhesion, addition of both acrylic acid and fibronectin dramatically improved cell adhesion and growth, and after 6 days of culture a confluent monolayer was observed (Fig 2B). We investigated the influence of PEG-DA on cell culture using hydrogels containing proportions of PEG-DA 700 varying from 30% up to 60% (Fig. S1). A minimum concentration of 30% (vol/vol) PEG-DA was necessary to permit Irgacure 819 solubilization and allow polymerization. We found that 40% of PEG-DA provided the best adhesion and proliferation for SW480 cells.

Comparisons of different ECMs, including fibronectin, collagen-1 and laminin were also performed. Results indicated that these three matrices similarly support cell adhesion and proliferation (Fig. 2C). Likewise, the optimal concentration of each matrix within the hydrogel was determined for SW480 cells (Fig. S2). Overall, fibronectin at 250 µg/mL was identified as the most favorable concentration for cell adhesion and was chosen for subsequent experiments. These results were confirmed with two other cell lines, Caco-2 (Fig. S3) and HeLa cells (data not

shown). Importantly, addition of fibronectin to PEG-DA hydrogel in absence of acrylic acid did not efficiently promote cell adhesion, and the presence of acrylic acid with fibronectin or laminin was necessary to allow cell adhesion and support cell growth for 6 days (Fig. S3). Thus, the retained hydrogel formulation for subsequent experiments was 40% PEG-DA 700 + 30% acrylic acid + 250 µg/mL fibronectin + 0.1% Irgacure 819 + 30 % culture medium.

It is difficult to provide a hierarchical ranking of the parameters influencing cell behavior. As a first hypothesis, the variation of the PEG-DA/acrylic acid ratio may influence the density of carboxylic acid groups available that in return promotes protein and cell adhesion. Another hypothesis is that cell proliferation could be affected by the mechanical and viscoelastic properties of the hydrogel scaffold. All these parameters are closely dependent on the material composition and their interplay may strongly influence cell proliferation and differentiation. Investigations are ongoing to decipher the influence of the PEG-DA/acrylic acid ratio on the material stiffness of the printed scaffold by Atomic Force Microscopy (AFM). Preliminary AFM data indicates a young modulus of 92 +/- 9.8 kPa for the selected hydrogel formulation (40% PEGDA, 30% acrylic acid and 250 µg/mL fibronectin). Interestingly, addition of fibronectin induced a significant stiffening of the resulting material with a young modulus value varying from 40 +/- 8.7 kPa for the PEG-DA/acrylic acid mix up to 90 kPa with fibronectin. This phenomenon may be explained by the interactions between fibronectin and the carboxylic groups provided by acrylic acid that induce a crosslinking effect in the matrix.

Fabrication of intestinal scaffolds

Three-dimensions scaffolds were printed using high-resolution stereolithography (SLA) 3D printing. The 3D printer (Dilase 3D, Kloe France) uses a 405 nm laser to print objects in a layer-by-layer building process [31]. Each individual scaffold measured 4x4 mm (x,y) with a total thickness of 0.75 mm. The topography was designed to reproduce the architecture and dimensions of the murine intestinal epithelium. Each single villus was surrounded by 6 crypts. Villi were 500 µm high, with a diameter of 150 µm at the top and 300 µm at the base. Crypt wells were 200 µm deep with a diameter of 50 µm (Fig. 3A). Intestinal scaffolds were printed on a DS3000 photoresist backplane to promote attachment of the hydrogel. We did not observe any noticeable cytotoxic effect of DS3000 on cell culture (data not shown). Scanning electron microscopy (SEM) images showed faithful replication of the design and reproducibility of the

printing (Fig. 3B). Dehydration of the hydrogel before SEM imaging resulted in partial collapse of the structures, impeding accurate measurement of the structures' dimensions. As PEG-DA is optically transparent in the visible range, 300 nm diameter fluorescent nanoparticles were added to the hydrogel to measure the 3D scaffold dimensions by two-photon microscopy and Light Sheet Fluorescence Microscopy (LSFM). Both imaging technologies allowed visualization of the villi of the scaffold. Although LSFM has an intrinsic resolution lower than two-photon imaging, it allows the visualization of a larger field including multiple rows of the scaffolds. Measures performed on two-photon images showed dimensions of 574 +/- 15 µm (n=10), compared to an initial programmed value of 500 µm. This expansion was confirmed on several samples observed showing a reproducible swelling of approximately 15%. This swelling effect may be related to the variation of pH (from 3.5 to 7.4) occurring between the fabrication process and the development step following printing. However, measures performed by LSFM showed high correspondence to the programmed dimensions (Fig. 3C-D). These differences of measurement may be explained by the fact that in LSFM, images are acquired from the side of the object and not from the top as in two-photon microscopy. Moreover, before imaging with LSFM, the sample was embedded in agarose, which may result in shrinking of the sample. Two-photon microscopy did not allow visualizing the crypt compartments, likely due to optical aberrations. Visualization of the crypt was possible by LSFM, but with a low resolution not allowing accurate measurements (Fig. 3D).

Suitability of 3D scaffolds for tissue culture

Three-dimensional hydrogel scaffolds supported adhesion and growth of Caco-2 cells. After 6 days of culture, a cell monolayer was observed around villi, with no cells inside the gel (Fig. 4A-C, E). LSFM imaging showed that the scaffold surface was not entirely covered by cells (Fig. 4C), indicating that 6 days of culture may not be sufficient for cells to proliferate and migrate to cover the entire structure uniformly. Focus on the crypt compartment by confocal imaging showed that cells also formed a continuous monolayer inside the crypt-like wells of the scaffold (Fig. 4D). However, we only observed cells down to a 72 +/- 4 µm depth. This value is significantly lower than the values of crypt depth measured before cell culture. We believe that the swelling effects observed earlier could result in a global compressive force and thus in a decrease of the crypt diameter that limits cell invasion within the structures. This swelling effect

could be compensated by adapting the STL file and increasing crypt diameter to obtain the correct dimensions in culture conditions.

Effect of 3D culture on cell differentiation

Caco-2 cells are known to differentiate spontaneously over time. After 21 days of culture they acquire properties similar to intestinal enterocytes and form a highly polarized epithelium with tight junctions [15, 46]. To study the impact of our 3D model on Caco-2 cell differentiation, we compared cells grown on various substrates for up to 21 days. First, the impact of the hydrogel was evaluated. Caco-2 cells were seeded on 2D hydrogel printed with the Dilase 3D or on glass coverslip, coated or not with fibronectin. F-Actin staining showed that Caco-2 cells formed a confluent monolayer in all three culture conditions (Fig. 5). However, cells grown on glass, coated or not with fibronectin, formed a highly flattened epithelium and exhibited no apico-basal polarization of nuclei or actin (Fig. 5A, B). On the contrary, cells that grew on 2D hydrogels exhibited an elongated morphology with apical actin and basal nuclei (Fig. 5C). Interestingly, cultures on 2D hydrogel reproducibly formed 3D structures, previously described as villi-like structures [47, 48]. For example, Fig. 5C shows a cross section of a 115 µm-high cellular structure displaying strong polarization of the actin network. This improved polarization of Caco-2 cells was not solely due to the presence of fibronectin in the hydrogel since cells that grew on fibronectin coated glass did not exhibit this characteristic morphology (Fig. 5B).

Polarization of Caco-2 cells was then evaluated on 3D intestinal scaffolds. High-resolution dynamic speckle imaging [43] allowed a complete visualization of the 3D scaffold and after 21 days of culture, cells had colonized it entirely, from the crypt base to the top of villi (Fig. 6A). Observation of the scaffold at 21 days showed that the structure had maintained its integrity and that the hydrogel was not degraded by cells (Fig. 6B). However, villi dimensions were significantly higher compared to measures obtained directly after printing (villi height = 728 +/- 64 µm after 21 days of culture, *n=10*), suggesting a progressive swelling of the gel over time (Fig. 6B). Monitoring of cellular morphology by F-actin staining showed that at 21 days post seeding, the epithelium was polarized, with apical actin and basal nuclei (visualized on the side of villi), while at 18 days of culture, the F-actin network was not fully organized yet (Fig. 6C, D). Caco-2 cells were previously shown to become more elongated during differentiation [49, 50]. Thus, we measured the height of cells cultivated on different substrates on vertical sections.

Interestingly, after 6 and 21 days of culture, cells grown on hydrogels (in 3D or 2D) were more elongated compared to cultures on glass coverslips (Fig. 6E), suggesting a better differentiation and confirming morphological observations. The presence of ECM in the hydrogel cannot explain this phenotype, as cells grown on fibronectin-coated glass exhibited poorly organized actin network and were less elongated than on 2D hydrogels (Fig. 6E). Cell length increased over time and was significantly higher in 3D at 21 days of culture compared to 6 days. However, only a slight elongation (< 3 µm) was observed on 2D hydrogels between 6 and 21 days of culture. Finally, there was a marked increase in cell length when grown on 3D scaffolds compared to 2D hydrogel, suggesting that the 3D topography provides cues promoting cell polarization that are not available in 2D (Fig. 6E).

To further evaluate the importance of 3D topography, we determined the influence of villus length on cell differentiation. For this, scaffolds were printed with 500 µm or µm high villi and seeded with Caco-2 cells for 21 days (Fig. S4). Monitoring of cell morphology with F-actin and β-catenin staining and cell height measurements did not reveal any difference and we observed a polarized epithelium with elongated cells, apical actin and membrane β-catenin in both conditions (Fig. S4 B-D). Thus, villi lengthening from 500 µm to 1500 µm does not appear to improve cell polarization.

Improved differentiation of cells grown on 3D scaffolds may be caused by distinct mechanical properties of the hydrogel, as well as surface topography and roughness. The latter was assessed by AFM and SEM imaging (Fig. S5). By SEM, the surface of the hydrogel was slightly uneven, with a regular motif probably caused by laser writing (Fig. S5 A, B). Measurements of surface topography by AFM revealed that the surface of 3D scaffolds was rougher than that of 2D hydrogels (Fig. S5 C, D). Indeed, measurements performed on cross sections indicated that the Rugosity average (Ra) was 419.3 nm for 3D hydrogel compared to a Ra = 85.78 nm for 2D hydrogel.

Differentiated absorptive enterocytes exhibit strong expression of villin, cytokeratin, phosphatase alkaline and membrane localization of β-catenin. The expression of differentiation markers by Caco-2 cells grown on 2D or 3D hydrogels was investigated after 21 days of culture (Fig. 7). As previously, cells exhibited strong apical F-actin staining in 3D, as well as extensive lateral

junction localization of β-catenin, while these were only observed on limited subsets of cells on 2D hydrogels (Fig. 7A). Similarly, cytokeratin staining gave abundant apicolateral signal on cells grown on 3D scaffolds compared to 2D hydrogels where it was restricted to the lateral junction of only a subpopulation of cells (Fig. 7B). Strikingly, Caco-2 cells grown on 3D scaffolds expressed villin and exhibited alkaline phosphatase activity, while it was absent or gave only weak staining in cells on 2D hydrogel (Fig 7 C, D), indicating that 3D topography provides additional cues that promote cellular differentiation, independently of the adhesion substrate. Interestingly, in 3D, villin and alkaline phosphatase staining were preferentially located towards the top of villi, suggesting a compartmentalization of the cells, with more differentiated cells located at the top of the villi, as observed *in vivo*. These results suggest that 3D architecture promotes cell differentiation and organization compared to 2D monolayer cultures.

Discussion

The intestinal epithelium presents a characteristic architecture with high aspect ratio villus and crypt compartments that exhibit distinct and intricate biochemical and biophysical environments. The existing *in vitro* systems, either 2D monolayer or 3D organoid cultures, do not faithfully reproduce this complex 3D microenvironment. Thus, over the last few years, intense efforts have been devoted to recreate this complex environment and recapitulate the topography of the small intestine for *in vitro* culture using microengineering approaches, with varying degrees of success [23, 51]. In this study, we developed a 3D scaffold mimicking the intestinal architecture using for the first time a PEG-DA/acrylic acid hydrogel enriched with fibronectin using a new 3D printing system [31].

We found that both the use of a hydrogel material and the micro-structuration of the surface with 3D topology is strongly influencing cell behavior. In fact, we showed that compared to traditional 2D cultures, Caco-2 cells grown on a 3D scaffold exhibit an improved differentiation and acquisition of an epithelial morphology with expression of enterocyte markers. These results indicate that the 3D morphology of the scaffold strongly impacts cell differentiation in our model, highlighting the importance of the 3D topography on cellular behavior. Other studies performing cultures on 3D scaffolds made with other materials or providing gradient biochemical stimulation similarly found that a 3D microenvironment promotes cell differentiation and offer a more physiologically relevant model to study the intestinal epithelium [16, 18, 21, 23].

As a proof of concept, the scaffold was made with a single hydrogel and a uniform environment. However, multiple gradients (growth factors, ECMs, oxygen, inflammatory signals…) have been described *in vivo* along the length of the crypt/villus axis [51]. For instance, concentrations of ECM proteins vary and adopt a specific distribution depending on the compartment. Indeed, different laminin subtypes are regionally expressed along the crypt/villus axis: laminin α2 is enriched in the crypts, while laminin α5 and α3 are expressed in villi [52, 53]. Laminin α5 was shown to play a crucial role in the maintenance of the mucosa and architecture, suggesting a relationship between ECM deposition and functional intestinal cell differentiation [54]. Other ECM proteins are also distributed regionally, including fibronectin, which is expressed preferentially in the crypt basement membrane [55]. Changes in ECM composition suggest

variations of stiffness, although it has not been directly measured *in vivo* due to technical limitations, and ECM mechanical properties are known to be important in the regulation of stem cell proliferation and fate [56]. A recent study using defined matrices for intestinal organoid cultures highlighted the importance of biochemical and biophysical roles of ECM in intestinal stem cell proliferation and differentiation [57]. Using customized PEG hydrogels, it was demonstrated that high matrix stiffness promotes ISCs expansion through YAP/Hippo pathway signaling, while soft and degradable matrices and the presence of laminin α1β1γ1 were needed for cell differentiation [41, 57]. For these reasons, it would be interesting to print 3D scaffolds using several hydrogels to recreate the different ECM composition to mimic these gradients along the crypt/villus axis and recapitulate more accurately the intestinal environment. Moreover, synthetic materials such as PEG-DA hydrogels are chemically and physically tunable, allowing their modification to modulate regional stiffness. In this work, we investigated the impact of both concentrations of PEG-DA and acrylic acid. We believe that the composition of the material may influence both the surface roughness and the mechanical properties, in particular the material's stiffness that could in return impact cell adhesion and proliferation. AFM measurements are currently in progress to investigate the correlation between cell culture results and the local stiffness sensed by the cells individually or when forming an epithelium.

Finally, gradients of soluble growth factors in the intestine are critical to control cell specification and proliferation. Among these, the Wnt/β-catenin pathway plays a crucial role for the maintenance and proliferation of intestinal stem cells [58], Wnt ligands are secreted by several crypt cells including Paneth cells and mesenchymal cells surrounding the crypts [59, 60]. Other signaling pathways that are essential in the crypt include Notch, BMPs and Eph/Ephrin [4]. Most of these signals are secreted by the mesenchymal compartment, which contains multiple cell populations [61]. These reports underscore the importance of the cellular niche in the intestinal environment and to fully recreate a physiological *in vitro* model, this cellular niche should be integrated. With recent progress in bioprinting, it is now possible to print 3D matrices containing cells [62]. With adequate materials and 3D printing technology, we can now envision printing 3D scaffolds mimicking the architecture of intestinal epithelium and containing supporting mesenchymal cells.

Conclusion

Herein, we describe a new 3D culture model mimicking the architecture of the intestinal epithelium. First, we developed a PEG-DA/acrylic acid hydrogel mix that supports cell adhesion and growth. This material is optically transparent, it exhibits a good compatibility with cell culture and can be easily tailored with a large variety of matrices. We then showed that this hydrogel mix can be advantageously combined with stereolithography to generate 3D scaffolds accurately recapitulating the intestinal topography. In addition, we showed by image analyses that compared to 2D cultures, cell culture on these 3D hydrogel scaffolds improved differentiation of Caco-2 intestinal epithelial cells. This 3D model could constitute an *in vitro* platform for studying fundamental mechanisms that drive intestinal homeostasis and regeneration. Beyond its application to intestinal tissues, the proposed approach provides a generic fabrication method that directly benefits from the flexibility of 3D printing technologies for the fabrication of 3D architectures with a resolution at the sub-cellular level. It opens new routes for the fabrication of *in vitro* microenvironment models with controlled topography either devoted to fundamental studies or used as standardized platforms for drug testing.

Acknowledgements

J.C. was supported by a studentship from the Region Midi-Pyrénées and Université Paul Sabatier – Toulouse III. This project was supported by funds from the Ligue Nationale Contre le Cancer, Fondation ARC pour la Recherche sur le Cancer and an “FRM Equipes” grant (DEQ20170336707) from the Fondation pour la Recherche Médicale to A.B.

This work was supported by the French RENATECH network. It was partly supported as part of the MuliFAB project funded by FEDER European Regional Funds and French Région Occitanie (grant agreement number 16007407/MP0011594) and by the HoliFAB project funded by the European Union's Horizon 2020 research and innovation program (grant agreement No 760927).

The authors thanks Sophie Allart and Danielle Daviaud (CPTP, Toulouse) for assistance with multiphoton imaging, Jacques Rouquette and Lise Teyssedre (ITAV, Toulouse) for LSFM imaging acquisitions and Brice Ronsin and Stephanie Bosch (CBI, Toulouse) for confocal imaging.

References

[1] N. Barker, Adult intestinal stem cells: critical drivers of epithelial homeostasis and regeneration, Nat Rev Mol Cell Biol 15(1) (2014) 19-33.
[2] N. Barker, J.H. van Es, J. Kuipers, P. Kujala, M. van den Born, M. Cozijnsen, A. Haegebarth, J. Korving, H. Begthel, P.J. Peters, H. Clevers, Identification of stem cells in small intestine and colon by marker gene Lgr5, Nature 449(7165) (2007) 1003-7.
[3] A.J.M. Santos, Y.H. Lo, A.T. Mah, C.J. Kuo, The Intestinal Stem Cell Niche: Homeostasis and Adaptations, Trends Cell Biol (2018).
[4] H. Clevers, The intestinal crypt, a prototype stem cell compartment, Cell 154(2) (2013) 274-84.
[5] X.C. He, J. Zhang, W.G. Tong, O. Tawfik, J. Ross, D.H. Scoville, Q. Tian, X. Zeng, X. He, L.M. Wiedemann, Y. Mishina, L. Li, BMP signaling inhibits intestinal stem cell self-renewal through suppression of Wnt-beta-catenin signaling, Nat Genet 36(10) (2004) 1117-21.
[6] H. Clevers, K.M. Loh, R. Nusse, Stem cell signaling. An integral program for tissue renewal and regeneration: Wnt signaling and stem cell control, Science 346(6205) (2014) 1248012.
[7] L.P. Pageot, N. Perreault, N. Basora, C. Francoeur, P. Magny, J.F. Beaulieu, Human cell models to study small intestinal functions: recapitulation of the crypt-villus axis, Microsc Res Tech 49(4) (2000) 394-406.
[8] M.A. Lancaster, J.A. Knoblich, Organogenesis in a dish: modeling development and disease using organoid technologies, Science 345(6194) (2014) 1247125.
[9] T. Sato, D.E. Stange, M. Ferrante, R.G. Vries, J.H. Van Es, S. Van den Brink, W.J. Van Houdt, A. Pronk, J. Van Gorp, P.D. Siersema, H. Clevers, Long-term expansion of epithelial organoids from human colon, adenoma, adenocarcinoma, and Barrett's epithelium, Gastroenterology 141(5) (2011) 1762-72.
[10] T. Sato, R.G. Vries, H.J. Snippert, M. van de Wetering, N. Barker, D.E. Stange, J.H. van Es, A. Abo, P. Kujala, P.J. Peters, H. Clevers, Single Lgr5 stem cells build crypt-villus structures in vitro without a mesenchymal niche, Nature 459(7244) (2009) 262-5.
[11] X. Yin, B.E. Mead, H. Safaee, R. Langer, J.M. Karp, O. Levy, Engineering Stem Cell Organoids, Cell Stem Cell 18(1) (2016) 25-38.
[12] J. Yu, R.L. Carrier, J.C. March, L.G. Griffith, Three dimensional human small intestine models for ADME-Tox studies, Drug Discov Today 19(10) (2014) 1587-94.
[13] S.N. Bhatia, D.E. Ingber, Microfluidic organs-on-chips, Nat Biotechnol 32(8) (2014) 760-72.
[14] G. Rossi, A. Manfrin, M.P. Lutolf, Progress and potential in organoid research, Nat Rev Genet (2018).
[15] I.J. Hidalgo, T.J. Raub, R.T. Borchardt, Characterization of the human colon carcinoma cell line (Caco-2) as a model system for intestinal epithelial permeability, Gastroenterology 96(3) (1989) 736-49.
[16] C.M. Costello, J. Hongpeng, S. Shaffiey, J. Yu, N.K. Jain, D. Hackam, J.C. March, Synthetic small intestinal scaffolds for improved studies of intestinal differentiation, Biotechnol Bioeng 111(6) (2014) 1222-32.
[17] C.M. Costello, R.M. Sorna, Y.L. Goh, I. Cengic, N.K. Jain, J.C. March, 3-D intestinal scaffolds for evaluating the therapeutic potential of probiotics, Mol Pharm 11(7) (2014) 2030-9.
[18] J. Yu, S. Peng, D. Luo, J.C. March, In vitro 3D human small intestinal villous model for drug permeability determination, Biotechnol Bioeng 109(9) (2012) 2173-8.
[19] Y. Chen, Y. Lin, K.M. Davis, Q. Wang, J. Rnjak-Kovacina, C. Li, R.R. Isberg, C.A. Kumamoto, J. Mecsas, D.L. Kaplan, Robust bioengineered 3D functional human intestinal epithelium, Sci Rep 5 (2015) 13708.

[20] M.B. Esch, J.H. Sung, J. Yang, C. Yu, J. Yu, J.C. March, M.L. Shuler, On chip porous polymer membranes for integration of gastrointestinal tract epithelium with microfluidic 'body-on-a-chip' devices, Biomed Microdevices 14(5) (2012) 895-906.
[21] J.H. Sung, J. Yu, D. Luo, M.L. Shuler, J.C. March, Microscale 3-D hydrogel scaffold for biomimetic gastrointestinal (GI) tract model, Lab Chip 11(3) (2011) 389-92.
[22] L. Wang, S.K. Murthy, W.H. Fowle, G.A. Barabino, R.L. Carrier, Influence of micro-well biomimetic topography on intestinal epithelial Caco-2 cell phenotype, Biomaterials 30(36) (2009) 6825-34.
[23] Y. Wang, D.B. Gunasekara, M.I. Reed, M. DiSalvo, S.J. Bultman, C.E. Sims, S.T. Magness, N.L. Allbritton, A microengineered collagen scaffold for generating a polarized crypt-villus architecture of human small intestinal epithelium, Biomaterials 128 (2017) 44-55.
[24] Y. Wang, R. Kim, D.B. Gunasekara, M.I. Reed, M. DiSalvo, D.L. Nguyen, S.J. Bultman, C.E. Sims, S.T. Magness, N.L. Allbritton, Formation of Human Colonic Crypt Array by Application of Chemical Gradients Across a Shaped Epithelial Monolayer, Cell Mol Gastroenterol Hepatol 5(2) (2018) 113-130.
[25] S.V. Murphy, A. Atala, 3D bioprinting of tissues and organs, Nat Biotechnol 32(8) (2014) 773-85.
[26] C. Mandrycky, Z. Wang, K. Kim, D.H. Kim, 3D bioprinting for engineering complex tissues, Biotechnol Adv 34(4) (2016) 422-434.
[27] R. Zhang, N.B. Larsen, Stereolithographic hydrogel printing of 3D culture chips with biofunctionalized complex 3D perfusion networks, Lab Chip 17(24) (2017) 4273-4282.
[28] A.P. Zhang, X. Qu, P. Soman, K.C. Hribar, J.W. Lee, S. Chen, S. He, Rapid fabrication of complex 3D extracellular microenvironments by dynamic optical projection stereolithography, Adv Mater 24(31) (2012) 4266-70.
[29] R. Gauvin, Y.C. Chen, J.W. Lee, P. Soman, P. Zorlutuna, J.W. Nichol, H. Bae, S. Chen, A. Khademhosseini, Microfabrication of complex porous tissue engineering scaffolds using 3D projection stereolithography, Biomaterials 33(15) (2012) 3824-34.
[30] K.C. Hribar, P. Soman, J. Warner, P. Chung, S. Chen, Light-assisted direct-write of 3D functional biomaterials, Lab Chip 14(2) (2014) 268-75.
[31] A. Accardo, R. Courson, R. Riesco, V. Raimbault, L. Malaquin, Direct laser fabrication of meso-scale 2D and 3D architectures with micrometric feature resolution, Additive Manufacturing 22 (2018) 440-446.
[32] E.A. Phelps, N. Landazuri, P.M. Thule, W.R. Taylor, A.J. Garcia, Bioartificial matrices for therapeutic vascularization, Proc Natl Acad Sci U S A 107(8) (2010) 3323-8.
[33] M.E. Smithmyer, L.A. Sawicki, A.M. Kloxin, Hydrogel scaffolds as in vitro models to study fibroblast activation in wound healing and disease, Biomater Sci 2(5) (2014) 634-650.
[34] J.J. Moon, M.S. Hahn, I. Kim, B.A. Nsiah, J.L. West, Micropatterning of poly(ethylene glycol) diacrylate hydrogels with biomolecules to regulate and guide endothelial morphogenesis, Tissue Eng Part A 15(3) (2009) 579-85.
[35] A. Urrios, C. Parra-Cabrera, N. Bhattacharjee, A.M. Gonzalez-Suarez, L.G. Rigat-Brugarolas, U. Nallapatti, J. Samitier, C.A. DeForest, F. Posas, J.L. Garcia-Cordero, A. Folch, 3D-printing of transparent bio-microfluidic devices in PEG-DA, Lab Chip 16(12) (2016) 2287-94.
[36] M. Verhulsel, M. Vignes, S. Descroix, L. Malaquin, D.M. Vignjevic, J.L. Viovy, A review of microfabrication and hydrogel engineering for micro-organs on chips, Biomaterials 35(6) (2014) 1816-32.
[37] M.P. Lutolf, J.A. Hubbell, Synthetic biomaterials as instructive extracellular microenvironments for morphogenesis in tissue engineering, Nat Biotechnol 23(1) (2005) 47-55.
[38] S.R. Caliari, J.A. Burdick, A practical guide to hydrogels for cell culture, Nat Methods 13(5) (2016) 405-14.

[39] D. Guarnieri, A. De Capua, M. Ventre, A. Borzacchiello, C. Pedone, D. Marasco, M. Ruvo, P.A. Netti, Covalently immobilized RGD gradient on PEG hydrogel scaffold influences cell migration parameters, Acta Biomater 6(7) (2010) 2532-9.
[40] R. Cruz-Acuna, M. Quiros, A.E. Farkas, P.H. Dedhia, S. Huang, D. Siuda, V. Garcia-Hernandez, A.J. Miller, J.R. Spence, A. Nusrat, A.J. Garcia, Synthetic hydrogels for human intestinal organoid generation and colonic wound repair, Nat Cell Biol 19(11) (2017) 1326-1335.
[41] N. Gjorevski, M.P. Lutolf, Synthesis and characterization of well-defined hydrogel matrices and their application to intestinal stem cell and organoid culture, Nat Protoc 12(11) (2017) 2263-2274.
[42] L. Chen, H.Z. An, P.S. Doyle, Synthesis of Nonspherical Microcapsules through Controlled Polyelectrolyte Coating of Hydrogel Templates, Langmuir 31(33) (2015) 9228-35.
[43] C. Ventalon, R. Heintzmann, J. Mertz, Dynamic speckle illumination microscopy with wavelet prefiltering, Opt Lett 32(11) (2007) 1417-9.
[44] J.W. Goodman, Speckle phenomena in optics: theory and applications, Roberts and Company Publishers2007.
[45] A. Accardo, M.C. Blatche, R. Courson, I. Loubinoux, C. Thibault, L. Malaquin, C. Vieu, Multiphoton Direct Laser Writing and 3D Imaging of Polymeric Freestanding Architectures for Cell Colonization, Small 13(27) (2017).
[46] M. Natoli, B.D. Leoni, I. D'Agnano, F. Zucco, A. Felsani, Good Caco-2 cell culture practices, Toxicol In Vitro 26(8) (2012) 1243-6.
[47] H.J. Kim, D. Huh, G. Hamilton, D.E. Ingber, Human gut-on-a-chip inhabited by microbial flora that experiences intestinal peristalsis-like motions and flow, Lab Chip 12(12) (2012) 2165-74.
[48] H.J. Kim, D.E. Ingber, Gut-on-a-Chip microenvironment induces human intestinal cells to undergo villus differentiation, Integr Biol (Camb) 5(9) (2013) 1130-40.
[49] M.D. Peterson, M.S. Mooseker, An in vitro model for the analysis of intestinal brush border assembly. I. Ultrastructural analysis of cell contact-induced brush border assembly in Caco-2BBe cells, J Cell Sci 105 (Pt 2) (1993) 445-60.
[50] E. Bazellieres, D. Massey-Harroche, M. Barthelemy-Requin, F. Richard, J.P. Arsanto, A. Le Bivic, Apico-basal elongation requires a drebrin-E-EB3 complex in columnar human epithelial cells, J Cell Sci 125(Pt 4) (2012) 919-31.
[51] Y. Wang, R. Kim, S.S. Hinman, B. Zwarycz, S.T. Magness, N.L. Allbritton, Bioengineered Systems and Designer Matrices That Recapitulate the Intestinal Stem Cell Niche, Cell Mol Gastroenterol Hepatol 5(3) (2018) 440-453 e1.
[52] L. Meran, A. Baulies, V.S.W. Li, Intestinal Stem Cell Niche: The Extracellular Matrix and Cellular Components, Stem Cells Int 2017 (2017) 7970385.
[53] I.C. Teller, J.F. Beaulieu, Interactions between laminin and epithelial cells in intestinal health and disease, Expert Rev Mol Med 3(24) (2001) 1-18.
[54] Z.X. Mahoney, T.S. Stappenbeck, J.H. Miner, Laminin alpha 5 influences the architecture of the mouse small intestine mucosa, J Cell Sci 121(Pt 15) (2008) 2493-502.
[55] Y.D. Benoit, J.F. Groulx, D. Gagne, J.F. Beaulieu, RGD-Dependent Epithelial Cell-Matrix Interactions in the Human Intestinal Crypt, J Signal Transduct 2012 (2012) 248759.
[56] F. Guilak, D.M. Cohen, B.T. Estes, J.M. Gimble, W. Liedtke, C.S. Chen, Control of stem cell fate by physical interactions with the extracellular matrix, Cell Stem Cell 5(1) (2009) 17-26.
[57] N. Gjorevski, N. Sachs, A. Manfrin, S. Giger, M.E. Bragina, P. Ordonez-Moran, H. Clevers, M.P. Lutolf, Designer matrices for intestinal stem cell and organoid culture, Nature 539(7630) (2016) 560-564.
[58] D. Pinto, A. Gregorieff, H. Begthel, H. Clevers, Canonical Wnt signals are essential for homeostasis of the intestinal epithelium, Genes Dev 17(14) (2003) 1709-13.
[59] A. Gregorieff, D. Pinto, H. Begthel, O. Destree, M. Kielman, H. Clevers, Expression pattern of Wnt signaling components in the adult intestine, Gastroenterology 129(2) (2005) 626-38.

[60] Z. Kabiri, G. Greicius, B. Madan, S. Biechele, Z. Zhong, H. Zaribafzadeh, Edison, J. Aliyev, Y. Wu, R. Bunte, B.O. Williams, J. Rossant, D.M. Virshup, Stroma provides an intestinal stem cell niche in the absence of epithelial Wnts, Development 141(11) (2014) 2206-15.
[61] D.W. Powell, I.V. Pinchuk, J.I. Saada, X. Chen, R.C. Mifflin, Mesenchymal cells of the intestinal lamina propria, Annu Rev Physiol 73 (2011) 213-37.
[62] L.R. Madden, T.V. Nguyen, S. Garcia-Mojica, V. Shah, A.V. Le, A. Peier, R. Visconti, E.M. Parker, S.C. Presnell, D.G. Nguyen, K.N. Retting, Bioprinted 3D Primary Human Intestinal Tissues Model Aspects of Native Physiology and ADME/Tox Functions, iScience 2 (2018) 156-167.

FIGURE LEGENDS

Figure 1: Schematic of the experimental strategy.

3D intestinal scaffolds were printed using a Dilase 3D high-resolution printer. The object is printed layer by layer of 20 to 50µm using a 405nm laser **(A-B)**. Scaffolds were then seeded with colorectal cancer cells that were grown for up to 21 days **(C)**.

Figure 2: Development of a new photosensitive hydrogel for tissue culture.

A. A mixture consisting of 40% PEG-DA 700 (v/v) and 30% acrylic acid (v/v) and Fibronectin in presence of Irgacure 819 was polymerized with UV light to form a hydrogel. **B.** Representative phase-contrast images of SW480 cells grown for 6 days on PEG-DA hydrogels containing or not acrylic acid and/or fibronectin. The bar graph shows the number of adherent cells per field (4 fields with a 20x objective counted from three independent experiments). **C.** Representative phase-contrast images of SW480 grown for 6 days on hydrogels containing different ECMs. Quantification was performed as in B. Scale bars = 50 µm.

Figure 3: 3D printing and imaging of intestinal scaffold.

A. CAD design and schematic of the 3D intestinal scaffold mimicking the topography and dimensions of murine intestinal epithelium. Numbers are in µm. Scaffolds were printed using a photopolymerizable hydrogel composed of 40% PEG-DA 700, 30% acrylic acid and 250 µg/ml fibronectin, fluorescent beads were added to visualize the scaffolds by fluorescence microscopy. **B**. SEM images of the 3D scaffold. **C**. 3D reconstructions (left and middle) and xz section (right) of the scaffold image by two-photon microscopy. **D**. Side view of the scaffold image (left) with Light Sheet Fluorescence Microscopy and 3D reconstruction (right). Scale Bars = 100 µm.

Figure 4: Cell culture on intestinal scaffolds.

Representative images of Caco-2 cells seeded on intestinal scaffolds. Cells were grown for 6 days fixed and then stained for DNA (Hoechst 33342, blue) and F-actin (FITC-Phalloidin, green). **A**. Two-photon imaging of the top, middle and base of the villi. Scale bars = 50 µm **B**. xz section of a single villus imaged by two-photon microscopy. **C**. Side view of the scaffold (top) and 3D reconstruction (bottom) of Light Sheet Fluorescence Microscopy acquisition. Scale bars

= 100 µm. **D**. xy and xz confocal microscopy images of the crypt compartment. Scale bars = 50 µm. **E**. Schematic showing the different horizontal cross-sections imaged on the 3D scaffold.

Figure 5: PEG-DA hydrogel induces apico-basal polarization of Caco-2 cells. Cells were plated on uncoated glass coverslips (A), glass coverslips coated with fibronectin (B), or on 2D hydrogel (C). After 21 days, cells were fixed and stained for F-actin with Phalloïdin- FITC (green) and nuclear DNA with DRAQ5 (blue). **A-B**. xy and xz view of Caco-2 cells cultured on uncoated glass coverslip (A) or fibronectin coated coverslips (B) for 21 days. **C**. Cellular morphology of Caco-2 cells grown on 2D PEG-DA/acrylic acid/fibronectin hydrogel for 21 days, 3D reconstruction of Z-stack imaging (lower left) and xz section (lower right) by confocal imaging. These experiments were realized on 3 independent samples. Scale bars = 50 µm.

Figure 6: Caco-2 cells form a polarized epithelium on 3D scaffold.
Cells were plated on 3D scaffold and after 18 or 21 days, cells were fixed and stained for nucleic acid (DRAQ5, blue) and F-actin (Phalloidin-FITC, green). **A**. 3D reconstruction of the scaffold by high-resolution dynamic speckle illumination imaging (left), focus on crypt level (middle) and xz section (right). **B**. Confocal imaging of villi xy section (left) and xz sections of the middle and base of a single villus (middle and right, respectively). **C-D**. Cellular morphology and actin polarization of cells cultured on 3D scaffolds for 18 and 21 days, respectively. These experiments were realized on 3 independent scaffolds. **E**. Average height of Caco-2 cells grown on 2D hydrogels or 3D scaffolds. Scale bar = 50 µm.

Figure 7: Caco-2 cells differentiates in 3 dimensions
Cells were seeded on 3D scaffolds or 2D hydrogels printed with the Dilase 3D. After 21 days of culture, cells were fixed and stained for F-actin, β-catenin, Pan-cytokeratin or villin. Nuclear DNA was stained with DRAQ5 (blue). **A.** Confocal imaging of β-catenin/F-actin co-staining on 2D or 3D hydrogels. **B.** Confocal imaging of Pan-cytokeratin staining (green) of Caco-2 grown on 2D or 3D hydrogels. **C.** xy and xz view of Caco-2 cells grown on 2D or 3D hydrogels stained for villin. **D.** Brightfield images of staining for alkaline phosphatase activity (blue) of Caco-2 grown on 2D or 3D hydrogels. Scale bars = 50 µm

Figure S1: Determination of optimal PEG-DA concentration.

Representative phase-contrast images of SW480 cells cultured for 6 days on various hydrogels. Bar graphs show the number of cells counted per field (4 fields with a 20x objective). Cell were grown on 30%, 40%, 50% and 60% PEG-DA 700 hydrogels ± acrylic acid ± fibronectin. Scale bars = 50 µm. Images and graph for the 40% condition are reproduced from Fig. 2B.

Figure S2: Optimization of ECM concentrations in hydrogels for tissue culture

Determination of the optimal concentrations of fibronectin (A), collagen-1 (B) or laminin (C) in 40% PEG-DA/30% acrylic acid hydrogels using SW480 cell cultured for 6 days on hydrogels. Graphs show the number of cells counted per field from 4 fields with a 20X objective. Scale bars = 50 µm.

Figure S3: Confirmation of the hydrogel with another colorectal cell line.

Representative fluorescence images of Caco-2 cells cultured on various hydrogels. Cells were seeded at 20,000 cells/cm^2, after 6 days of culture, cells were fixed and stained for F-actin with phalloïdin-FITC and nuclear DNA was stained with Hoechst 33342. The bar graph shows the quantification of cells number per field (40X, 4 fields counted). Scale bars = 25 µm.

Figure S4: Influences of villi length on cellular behavior

(A) SEM images of 3D scaffolds of 500 µm and 1500 µm high villi. (B, C) Representative confocal images of Caco-2 cells grown on 500 µm (B) or 1500 µm (C) high villi. Cells were grown for 21 d, fixed and stained for F-actin (Phalloidin-rhodamine, red), β-catenin (green) and nuclear DNA (DRAQ5, blue). (D) Average height of Caco-2 cells grown on 3D scaffolds with 500 µm or 1500 µm high villi.

Figure S5: Surface topography and roughness of the hydrogel

(A, B) Representative SEM images of 2D (A) or 3D (B) hydrogels. (C, D) AFM imaging of 2D (C) or 3D (D) hydrogels. Cross section and 3D view is presented for each sample.

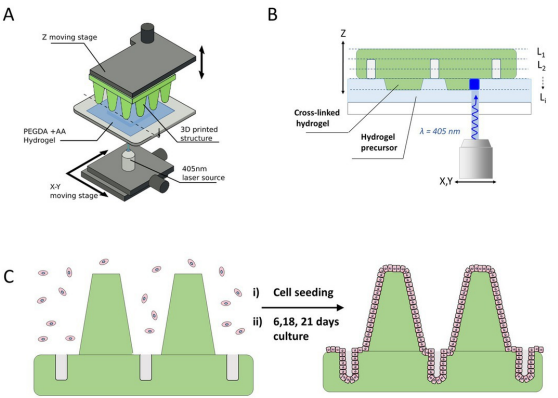
A
Z moving stage
PEGDA +AA
Hydrogel
3D printed
structure
405nm
laser source
X-Y
moving stage
B
Z
L1
L2
Ln
Cross-linked
hydrogel
Hydrogel
precursor
λ = 405 nm
X,Y
C
i) Cell seeding
ii) 6,18, 21 days
culture

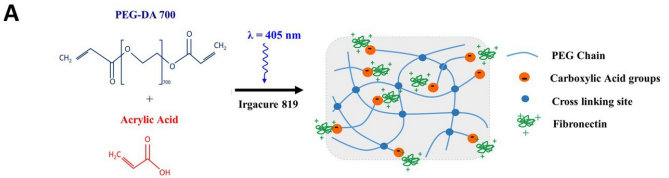
A
PEG-DA 700
λ = 405 nm
Irgacure 819
Acrylic Acid
PEG Chain
Carboxylic Acid groups
Cross linking site
Fibronectin

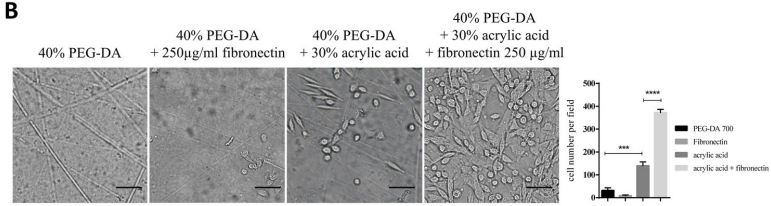
B
40% PEG-DA
40% PEG-DA + 250µg/ml fibronectin
40% PEG-DA + 30% acrylic acid
40% PEG-DA + 30% acrylic acid + fibronectin 250 µg/ml
cell number per field
***
****
PEG-DA 700
Fibronectin
acrylic acid
acrylic acid + fibronectin

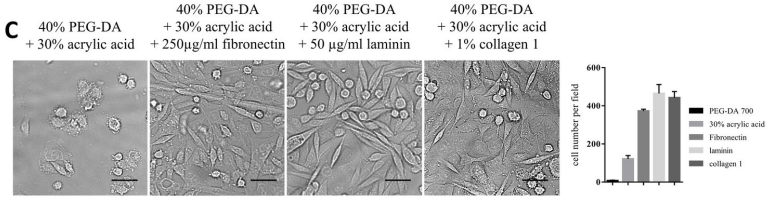
C
40% PEG-DA + 30% acrylic acid
40% PEG-DA + 30% acrylic acid + 250µg/ml fibronectin
40% PEG-DA + 30% acrylic acid + 50 µg/ml laminin
40% PEG-DA + 30% acrylic acid + 1% collagen 1
cell number per field
PEG-DA 700
30% acrylic acid
Fibronectin
laminin
collagen 1

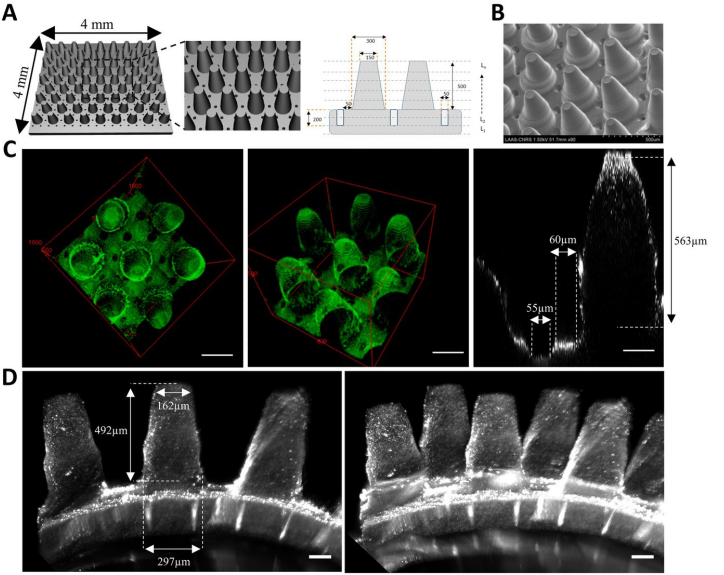
A
4 mm
4 mm
300
150
500
200
B
C
60µm
55µm
563µm
D
162µm
492µm
297µm

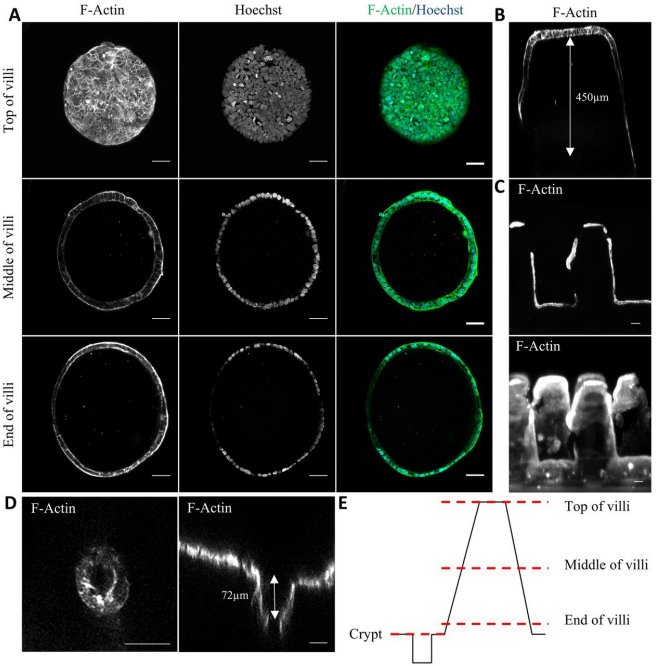
A
F-Actin
Hoechst
F-Actin/Hoechst
Top of villi
Middle of villi
End of villi
B
F-Actin
450μm
C
F-Actin
F-Actin
D
F-Actin
F-Actin
72μm
E
Top of villi
Middle of villi
End of villi
Crypt

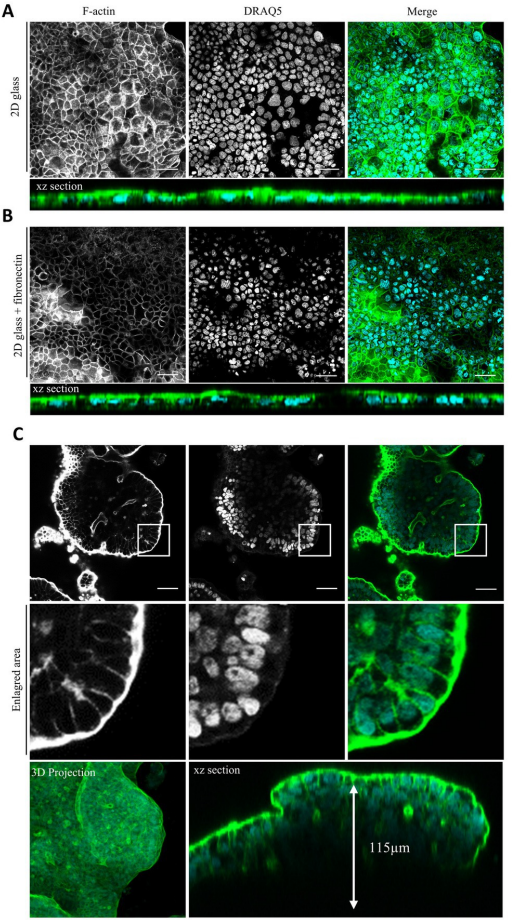
A
F-actin
DRAQ5
Merge
2D glass
xz section
B
2D glass + fibronectin
xz section
C
Enlagred area
3D Projection
xz section
115µm

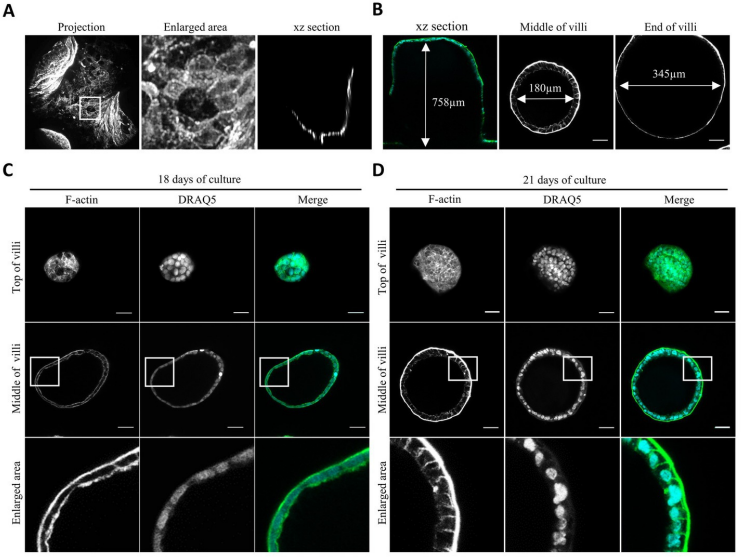
A
Projection
Enlarged area
xz section
B
xz section
Middle of villi
End of villi
758µm
180µm
345µm
C
18 days of culture
F-actin
DRAQ5
Merge
Top of villi
Middle of villi
Enlarged area
D
21 days of culture
F-actin
DRAQ5
Merge
Top of villi
Middle of villi
Enlarged area

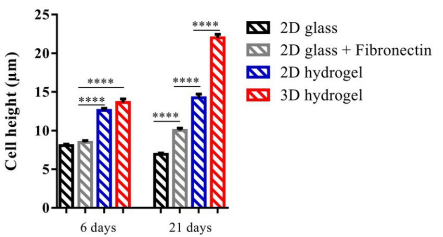
E
Cell height (µm)
25
20
15
10
5
0
****
****
****
****
6 days
21 days
2D glass
2D glass + Fibronectin
2D hydrogel
3D hydrogel

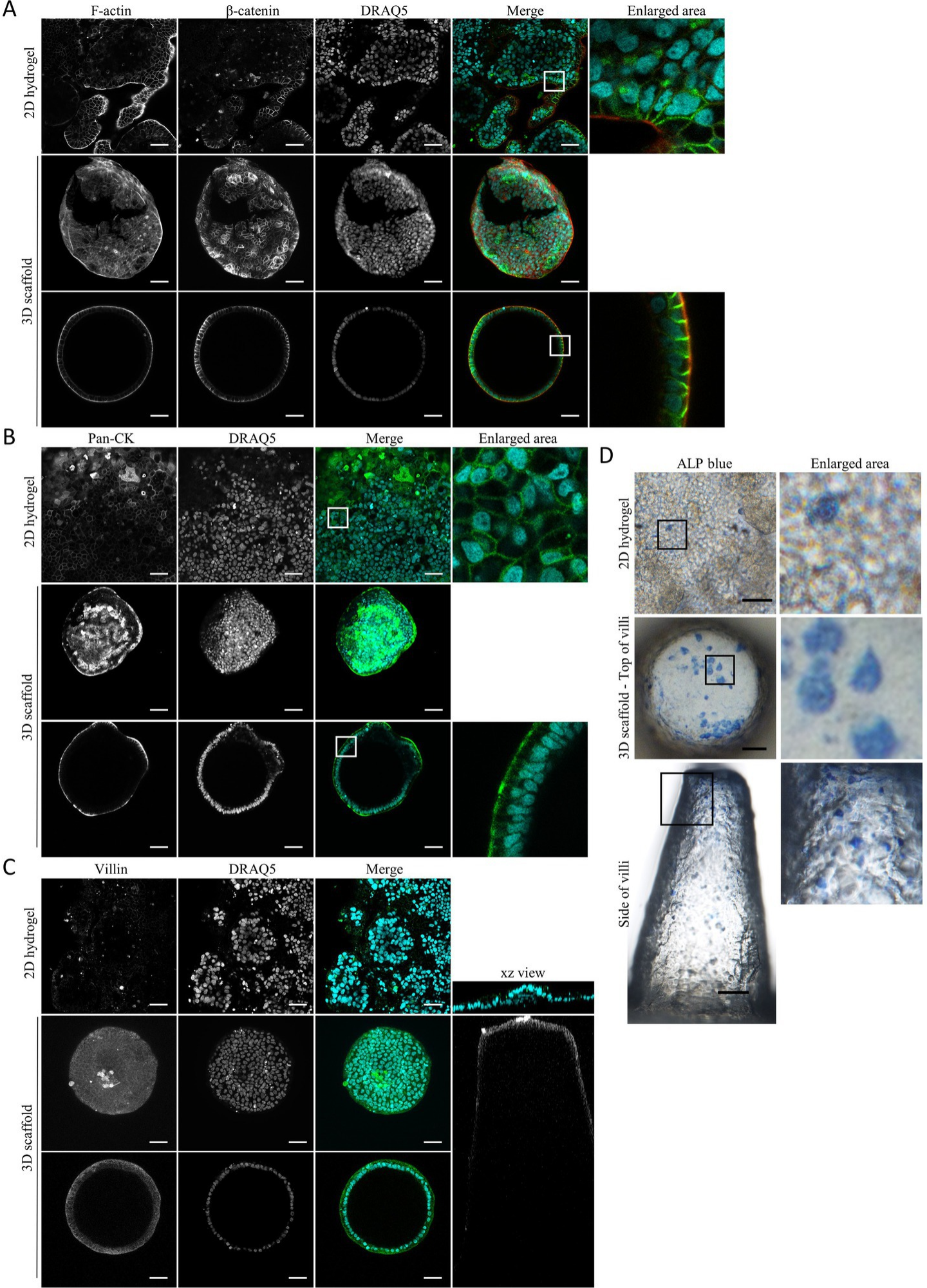
A
F-actin
β-catenin
DRAQ5
Merge
Enlarged area
2D hydrogel
3D scaffold
B
Pan-CK
DRAQ5
Merge
Enlarged area
2D hydrogel
3D scaffold
C
Villin
DRAQ5
Merge
xz view
2D hydrogel
3D scaffold
D
ALP blue
Enlarged area
2D hydrogel
3D scaffold - Top of villi
Side of villi